energy&fuels

pubs.acs.org/EF

Article

Polyethylene Oxide/Sodium Sulfonamide Polymethacrylate Blends as Highly Conducting Single-Ion Solid Polymer Electrolytes

Jorge L. Olmedo-Martínez, Asier Fdz De Anastro, María Martínez-Ibañez, Alejandro J. Müller,* and David Mecerreyes*

Cite This: *Energy Fuels* 2023, 37, 5519−5529

Read Online

ACCESS | Metrics & More | Article Recommendations | Supporting Information

ABSTRACT: In this work, blends of polyethylene oxide (PEO) and poly(sodium 1-[3-(methacryloyloxy)propylsulfonyl]-1-(trifluoromethanesulfonyl) imide) (PNaMTFSI) in different compositions were investigated for their application as solid electrolytes for sodium batteries. PNaMTFSI and PEO are miscible, exhibiting only one T_g in the whole range of compositions. PNaMTFSI was shown to reduce the crystal growth rate of PEO crystals but increase PEO nucleation, making the overall crystallization rate higher in blends with 15 and 30 wt % PNaMTFSI. The ionic conductivity is also affected by the blend composition. The highest values of ionic conductivity were observed with 15 and 30 wt % PNaMTFSI at high temperatures equal to 5.84×10^{-5} and 7.74×10^{-5} S cm^{-1} at 85 °C, respectively, with values of sodium-ion transference numbers of higher than 0.83 and electrochemical stability between 3.5 and 4.5 V versus Na^+/Na^0 depending on the composition, which opens the possibility of its use in sodium batteries. Finally, a comparison was made between the effect of sodium and lithium on these types of electrolytes, showing that sodium electrolytes have a lower ionic conductivity due to the larger size of the Na cation. The differences in the spherulitic growth rate and overall crystallization rate between Li and Na-containing electrolytes were compared and rationalized in terms of the blends' intermolecular interactions and the relative contribution of primary nucleation and growth.

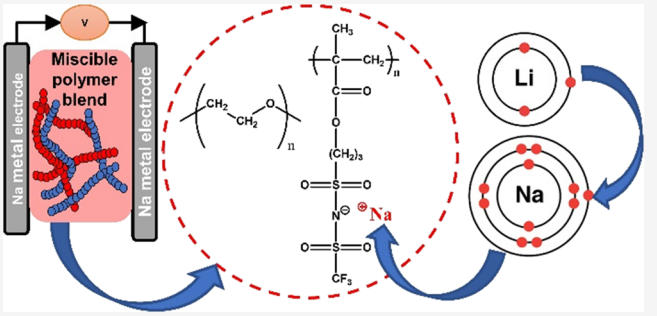

1. INTRODUCTION

Rechargeable batteries are in high demand as one of the most widely used energy storage devices in electronic appliances and electric cars.[1,2] Currently, these batteries are based on lithium;[3] however, its limited availability and its price are becoming limiting factors. For these reasons, there is currently an interest in switching to sodium batteries since sodium is a more abundant element and has a lower price than lithium.[4] Sodium presents similarities with lithium for batteries, showing a high specific capacity (1166 mAh g^{-1}) and a low redox potential (−2.71 V vs standard hydrogen electrode).[5] However, sodium batteries present still some limitations, including low performance and safety issues.

One of the key components for optimal battery performance is the electrolyte, which must be an electrical insulator and a good ionic conductor to transport the ions from one electrode to another. Typically, liquid electrolytes are used for lithium or sodium batteries since they present high ionic conductivity. Still, they have certain problems, for example, dendrite growth, leakage, and the use of organic solvents that are usually toxic and flammable (e.g., ethylene carbonate and dimethyl carbonate) among others.[6] Solid electrolytes based on polymers are safer since there is no risk of leakage, and they are more resistant to dendrite growth.[7] Solid polymer electrolytes (SPEs) are the main type of solid electrolyte where only polymers are included without the need of an additional low molecular weight plasticizer as in the case of gel polymer electrolytes (GPEs) or inorganic particles as in hybrid solid electrolytes. Despite their lower ionic conductivity, SPEs are preferred for their higher mechanical modulus compared to GPEs, which show a beneficial effect in avoiding metal dendrite growth.

Ion transport in SPEs depends on the ability of ions to move between ion coordination sites. The most studied host matrix in SPEs is polyethylene oxide (PEO) for its capacity to dissolve different salts.[8] The ionic conduction in PEO involves the arrangement of polymer chain segments, creating dynamic coordination sites where both cations and anions can move, allowing their movement.[9] Recently, single-ion conducting systems have been investigated for application in lithium metal batteries where the movement of the cation is the only one

Received: December 23, 2022
Revised: March 12, 2023
Published: March 27, 2023

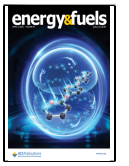

Scheme 1. (a) Ion Exchange for Obtaining the Sodium Monomer and (b) Obtaining the PNaMTFSI Polymer by RAFT Polymerization

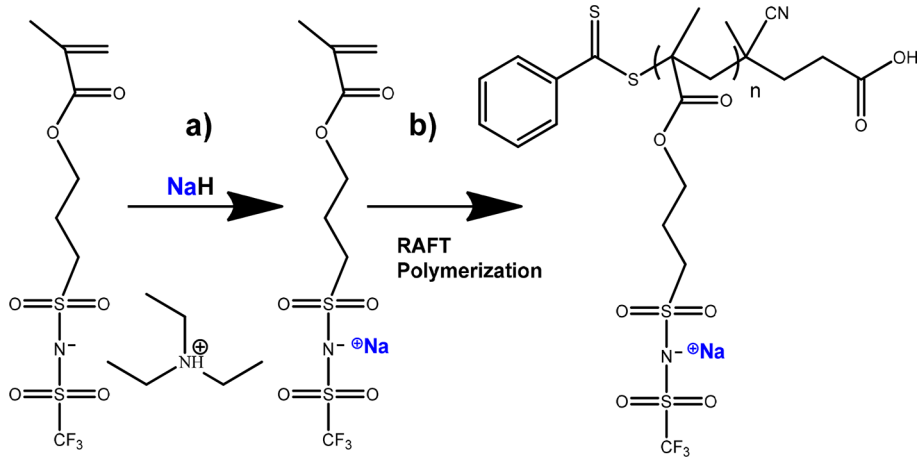

that participates in the conduction process. This, in the case of polymeric electrolytes, is achieved by attaching the anion to the polymeric chain through an anionic polymer backbone. The advantage of using single-ion polymer electrolytes is that the lithium-ion transference number is close to 1, indicating that the ionic conductivity is only due to the movement of cations.[10,11] Under these conditions, ion concentration polarization is avoided and high-power performance is achieved, which reduces dendritic growth.[12,13]

Single-ion-conducting polymer electrolytes have been studied extensively for lithium batteries, but only a few works have been published using sodium single-ion polymer electrolytes for sodium batteries, delivering ionic conductivity values in the range of 10^{-8}–10^{-5} S cm^{-1}.[14−16] For example, Liu et al. reported an electrolyte based on sodium bis(fluoroallyl)malonate borate salt (NaBFMB), which was photo-cross-linked with tri-thiol trimethylolpropane tris(3-mercapto propionate) (TMPT);[17] this electrolyte was shown to have a sodium transport number of 0.91 in addition to good electrochemical stability and ionic conductivity in the order of 10^{-3} S cm^{-1} at 30 °C. Armand et al. synthesized a single-ion polymer electrolyte by grafting silica (SiO_2) nanoparticles with sodium 2-[(trifluoromethane-sulfonylimido)-*N*-4-sulfonylphenyl]ethyl and/or poly(ethylene glycol monomethyl ether) (PEG) strands and obtained ionic conductivities of 2×10^{-5} S cm^{-1} at 25 °C.[18] However, in these cases, complex synthesis techniques or the incorporation of inorganic nanoparticles was used.

In this work, polymer blending as an inexpensive and practical technique for the development of materials[19] was employed to develop sodium single-ion conducting polymer electrolytes. The successful strategy of high-conducting single-ion conducting polymer blends for lithium metal batteries has been previously reported.[20−23] Here, we applied a similar method to the design of sodium single-ion polymer electrolytes with high conductivity. Thus, single-ion polymer electrolytes were prepared by blending polyethylene oxide (PEO) and poly(sodium 1-[3-(methacryloyloxy) propylsulfonyl]-1-(trifluoromethanesulfonyl) imide) (PNaMTFSI). An important property of this polymer (PNaMTFSI) is that the negative charge on the fluorinated alkyl sulfonyl imide anion is highly dispersed by the conjugated delocalization of the sulfonyl imide group and the strong electron-pulling of the fluorinated group, and such anions usually exhibit strong delocalization, which allows the cation (sodium in this case) to be easily solvated by the oxygens present in the PEO. Solid polymer electrolyte films were prepared by varying the concentration of PNaMTFSI, and the effect of this polymer on PEO crystallization as well as on the ionic conductivity was investigated. Finally, the stability of these solid electrolytes with respect to sodium metal electrodes was evaluated.

2. EXPERIMENTAL SECTION

2.1. Materials. The following materials were used: polyethylene oxide (PEO with an M_v value of 100 kg mol^{-1}; Sigma-Aldrich), 3-sulfopropyl methacrylate potassium salt (98%; Sigma-Aldrich), 4-cyano-4-(phenylcarbonothioylthio) pentanioc acid (CPADB >97%; Sigma-Aldrich), dichloromethane (DCM; Across), sodium hydrate (NaH, 90%; Sigma-Aldrich), tetrahydrofuran (THF; Across), 2,2′-azobis(2-methylpropionitrile) (AIBN >98%, initiator; Sigma-Aldrich), *N*,*N*-dimethylformamide (DMF; Across), Milli-Q water, and sodium metal (sticks; PANREAC, 99.8%).

2.2. Synthesis of Poly(sodium 1-[3-(methacryloyloxy) propylsulfonyl]-1-(trifluoromethanesulfonyl) imide) (PNaMTFSI). The NaMTFSI monomer was synthesized by the procedure reported by Shaplov et al.[24,25] Obtaining the monomer consisted of three steps. In the first stage, potassium 3-(methacryloyloxy)propane-1-sulfonate was converted into the sulfonyl chloride derivative by a reaction with thionyl chloride in the presence of DMF as a catalyst. The second stage consisted the reaction of the product obtained in the first stage with trifluoromethanesulfonamide in the presence of an excess of triethylamine. In the third step, the reaction proceeds with NaH to eliminate free thriethylamine and to substitute the thriethylammonium cation with the sodium one (see Scheme 1a).

PNaMTFSI was prepared by reversible addition-fragmentation chain-transfer (RAFT) polymerization to obtain a polymer with a molecular weight (M_n) of ∼50 kg mol^{-1} (Scheme 1b). A degassed solution of NaMTFSI (1.5 g), CPADB (8.5 mg), and AIBN (1 mg) in 5 g of DMF with a magnetic stir bar was placed in a Schlenk tube. The polymerization reaction was carried out at 70 °C for 24 h under an argon atmosphere, and the reaction yield was 80%. The polymer solution was put in a roto-evaporator to remove DMF and then dissolved in 5 g of methanol and finally precipitated in DCM; this procedure was repeated twice. After purifying the polymer, its color went from pink to red (due to the intense red color of the CTA agent used). Figure S1 presents the ^{1}H NMR data of PNaMTFSI. When PNaMTFSI was completely dry, it was rigid.

2.3. PEO/PNaMTFSI Blend Preparation. The polymer electrolyte blends were prepared by a solvent-casting method. The polymers were dissolved in water, and four different compositions were

https://doi.org/10.1021/acs.energyfuels.2c04296
Energy Fuels 2023, 37, 5519−5529

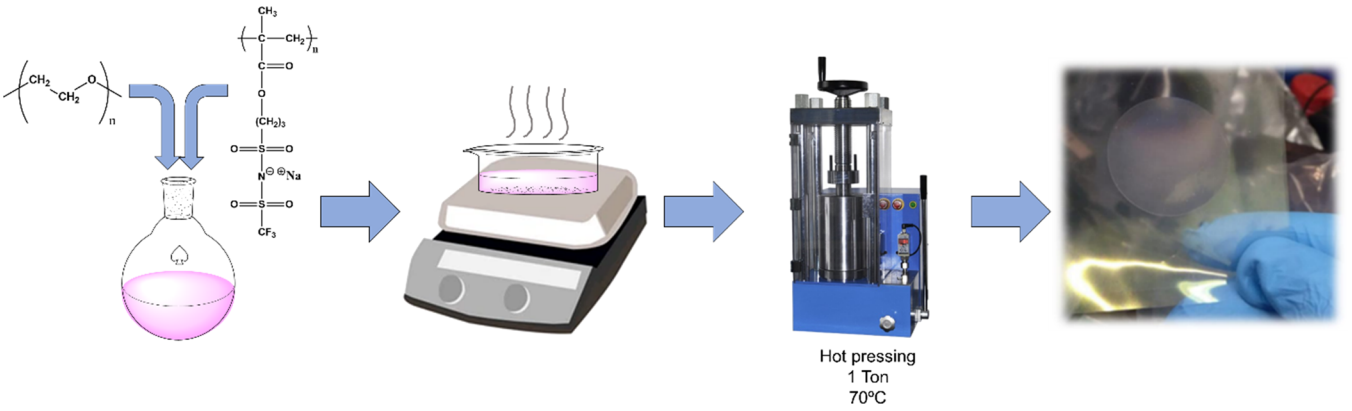

Figure 1. Preparation process of the polymer electrolyte blends.

prepared for PNaMTFSI in PEO (15, 30, 50, and 70 wt %). After evaporating the water at room temperature, the electrolytes were completely dried under vacuum at 70 °C for 12 h. Finally, the electrolyte films were compression-molded in a press at 70 °C and 1 ton of pressure; the process is shown in Figure 1. The films obtained are transparent with a slightly pink color, as shown in the final step of Figure 1.

2.4. Characterization Methods. The electrolytes were studied by differential scanning calorimetry (DSC). A PerkinElmer 8000 DSC fitted with an Intracooler II with a nitrogen atmosphere was used for the experiments. The equipment was calibrated with indium and tin standards. The samples for non-isothermal and isothermal experiments were placed in aluminum pans, and the mass employed in all cases was approximately 5 mg. For the non-isothermal experiments, a range between −60 and 100 °C was used. The first heating scan was used to erase the thermal history of the material; then, it was cooled down to −60 °C and then heated again to 100 °C. The cooling and second heating scans were employed for the analysis of the non-isothermal results. The heating and cooling rates were 20 °C min^{-1}.

The crystallization temperatures (T_c) employed for the isothermal crystallization experiments were obtained using the methodology proposed by Lorenzo et al. and Pérez-Camargo et al.[26,27]

The procedure for the isothermal crystallization experiments was as follows: (1) heat the sample from 25 to 100 °C at 20 °C min^{-1}, (2) hold for 3 min at 100 °C, (3) cool to T_c at 60 °C min^{-1}, (4) hold at T_c for 40 min to allow PEO crystallization, and then (5) heat from T_c to 100 °C at 20 °C min^{-1} to measure the melting temperature change as a function of T_c.

The PEO crystallinity degree was calculated using the equation

$$X_c = \frac{\Delta H_m}{f \Delta H_m^0} \times 100 \quad (1)$$

where ΔH_m is the measured melting enthalpy, ΔH_m^0 is the equilibrium melting enthalpy (for PEO, it is 214 J g^{-1}),[28] and f is the PEO weight fraction in the sample.

The glass transition temperature (T_g) in a temperature sweep in the DSC is observed as a stepwise endothermic change in the heat flow. This value is taken at the midpoint of this change. The Gordon-Taylor equation was employed to fit the change in T_g with respect to the composition[29]

$$T_{g,blend} = \frac{w_1 T_{g1} + k w_2 T_{g2}}{w_1 + k w_2} \quad (2)$$

where w_1 and w_2 are the polymer component weight fractions, T_{g1} and T_{g2} are the glass transition temperatures of PEO and PNaMTFSI, respectively, and k is the $\rho_1 \Delta\alpha_2 / \rho_2 \Delta\alpha_1$ ratio. ρ and $\Delta\alpha$ correspond to the density and the expansion coefficient change at T_g, respectively.[30]

The ionic conductivity was determined by electrochemical impedance spectroscopy (EIS) using an Autolab 302N potentiostat galvanostat. The experiments were carried out at different temperatures (95−25 °C). The electrolyte was placed between two stainless steel electrodes (surface area = 0.5 cm^2). The Nyquist plots were obtained in the 100 kHz to 1 Hz range with a 10 mV amplitude.

The Vogel−Tammann−Fulcher (VTF) equation was used to adjust the ionic conductivity values of the electrolytes in order to calculate the activation energies[31]

$$\sigma = A \exp\left(\frac{-E_a}{R(T - T_0)}\right) \quad (3)$$

where A is the prefactor of the equation, which has the same unit as the ionic conductivity (S cm^{-1}), R is the universal gas constant (8.314 J mol^{-1} K^{-1}), T is the temperature in Kelvin, and T_0 is the Vogel temperature (T_g − 50 °C).

The sodium-ion transference number (t_{Na^+}) was determined by a combined measurement of AC impedance and DC polarization until a steady state current was obtained after 12 h using a Multi Potentiostat VMP3 (Biologic, France) at 70 °C. For this purpose, a CR2032-type coin cell was used using two Na^0 disk electrodes (Na^0|PE|Na^0) assembled under an argon atmosphere in a glovebox. The impedance spectra were recorded in the frequency range of 1 MHz to 0.1 Hz using an amplitude of 10 mV before and after DC polarization.

The sodium-ion transference number was determined using the Bruce and Vincent method using the following equation[32]

$$t_{Na^+} = \frac{I_f(\Delta V - I_0 R_{i,0})}{I_0(\Delta V - I_f R_{i,f})} \quad (4)$$

where ΔV is the applied DC voltage, I_0 and I_f are the initial and steady-state currents, and $R_{i,f}$ and $R_{i,0}$ are the steady-state and initial resistance at the Na^0|PE interface, respectively.

The spherulitic growth rate and morphology were obtained using an OLYMPUS BX51 polarized light optical microscope (PLOM) fitted with an OLYMPUS SC50 camera and a Mettler FP82HT hot stage with a liquid-nitrogen cooling capability. The electrolyte samples were placed between two glass slides and heated until 100 °C to form a thin film and kept at this temperature for 3 min to erase thermal history. Afterward, the sample was cooled at 50 °C min^{-1} to a temperature at which the spherulites began to appear. Ten photographs were taken as a function of time for 10 T_c values. By plotting the radius of the spherulite as a function of time, a straight line was always obtained, and the slope gave the spherulitic growth rate.

Linear sweep voltammetry (LSV) experiments were performed using a CR2032-type coin cell. These cells were assembled comprising a stainless steel working electrode and Na^0 disk as both the reference and counter electrode inside the argon-filled glovebox. Measurements were performed between the open-circuit potential (OCV) and 6.0 V versus Na^+/Na^0 at a scan rate of 1 mV s^{-1} using a Multichannel Potentiostat VMP3 (BioLogic, France).

Na^0 symmetrical coin cells (Na^0|PE|Na^0) were assembled inside an argon-filled glovebox and used to study the evolution of the total

https://doi.org/10.1021/acs.energyfuels.2c04296
Energy Fuels 2023, 37, 5519−5529

resistance over the temperature from 25 to 70 °C using a Multi Potentiostat VMP3 (Biologic, France).

Cyclic voltammetry (CV) experiments were performed using CR2032-type coin cells. These cells were assembled comprising a copper working electrode and Na^0 disk as both the reference and counter electrode inside the argon-filled glovebox. Measurements were performed between the open-circuit potential (OCV) and −1.0 V versus Na^+/Na^0 at a scan rate of 1 mV s^{-1} using a Multichannel Potentiostat VMP3 (BioLogic, France). The Coulombic efficiency of the plating/stripping process was determined using the following equation

$$\mathrm{CE}(\%) = \frac{C_{\mathrm{plat.max.}} - C_{\mathrm{plat0}}}{C_{\mathrm{strip.max.}} - C_{\mathrm{strip0}}} \quad (5)$$

where $C_{\mathrm{plat.\ max\ .}}$ and C_{plat0} are the maximum and initial plating currents and $C_{\mathrm{strip.\ max\ .}}$ and C_{strip0} are the maximum and initial striping currents given in percentage, respectively.

3. RESULTS AND DISCUSSION

Polymer blends were prepared in different compositions. PNaMTFSI of ∼50,000 g mol^{-1} was synthesized by RAFT polymerization as described in the Experimental Section, and PEO of 100,000 g mol^{-1} was used. These polymer molecular weights were chosen because they showed the highest values in terms of ionic conductivity for lithium single-ion polymer blends.[22] First, both homopolymers were dissolved together in water. After evaporating the solvent and drying the polymer blend extensively, the polymer films were prepared in a hot press as shown in Figure 1 (the storage modulus as a function of the temperature for the blends is presented in Figure S2).

3.1. Non-isothermal DSC. First, we investigated the blends by DSC. Ion transport in a polymeric host is influenced by the crystallinity and segmental movement of the polymeric chains. Ionic conductivity takes place preferentially in the amorphous phase of the polymer matrix, and thus, crystallinity will restrict the ion mobility. Moreover, polymers with lower glass transition temperatures (T_g) are characterized by higher long-range segmental movements (above T_g), increasing the ionic conductivity.[33,34] For this reason, the results obtained from DSC and ionic conductivity measurements are usually correlated. PNaMTFSI is an amorphous polymer with a T_g of 97 °C,[22] while PEO is a semi-crystalline one with a T_m of 68 °C and a T_g of −55 °C, and these values coincide with those reported in the literature.[25]

Figure 2a shows the DSC curves for neat PEO and the electrolytes. It is observed that the melting temperature of PEO decreases from 68 to 65 °C with the addition of 30 wt % PNaMTFSI (blend 70/30). Upon the addition of 50 and 70 wt % PNaMTFSI (50/50 and 30/70), the PEO phase is rendered amorphous. Additionally, the crystallinity of PEO (X_c) decreases from 60 to 45% with 30 wt % PNaMTFSI (70/30). On the other hand, the T_g increases as the amount of PNaMTFSI in the electrolyte increases. This effect is clearly seen in electrolytes with a high concentration of PNaMTFSI as, with 50 wt %, the T_g is −18.9 °C and, with 70 wt %, it is 0.4 °C.

Figure 2b represents the experimental T_g as a function of the PEO fraction, and the Gordon-Taylor equation allows the prediction of the T_g of the blend from the T_g's of the individual polymers, assuming that both polymers are miscible. For the samples that are completely amorphous (50/50 and 30/70), a very clear T_g is observed, and these values fit the Gordon-Taylor equation very well, indicating that the polymers are miscible; for the electrolytes with a lower concentration of PNaMTFSI (85/15 and 70/30), the PEO maintains crystallinity and the change in T_g is not very clear. However, the T_g value for these blends can be predicted with the Gordon-Taylor equation. These results indicate that PEO and PNaMTFSI are miscible. A similar result was also obtained for the PEO/PLiMTFSI blend reported before.[22]

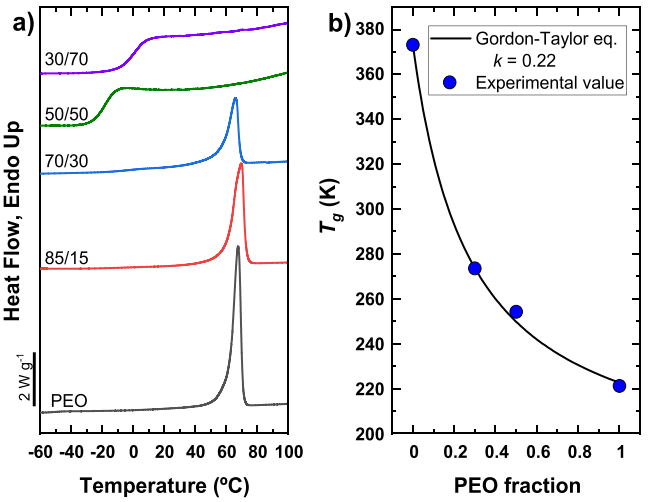

Figure 2. (a) Second heating DSC curves for neat PEO and the prepared PEO/PNaMTFSI blends, (b) T_g as a function of the PEO fraction; the blue dots are the experimental T_g obtained by DSC, and the solid black line is the fit of the Gordon-Taylor equation.

3.2. Isothermal Crystallization and Morphology. The morphology and spherulitic growth rate were evaluated with a polarized light optical microscope (PLOM). Figure 3 shows the morphology of the PEO semi-crystalline superstructures at an isothermal crystallization temperature of 50 °C for neat PEO (Figure 3a) and for the blends 85/15 and 70/30 (Figure 3b,c, respectively). For neat PEO, large negative spherulites were observed with very clear Maltese cross extension patterns. On the other hand, the PEO spherulites in the blends with 15% PNaMTFSI exhibit much smaller spherulites (see Figure 3b and notice the different scale bar with respect to Figure 3a). This indicates that the PNaMTFSI diluent increased the nucleation density of PEO and also the morphology of the spherulites changed as the Maltese cross pattern is difficult to observe. Increasing the concentration of PNaMTFSI to 30% distorts the PEO spherulites, and the nucleation increases even further. Changes in the spherulite morphology and increased nucleation are further evidence of miscibility between the polymers. The increase in the nuclei density may be due to the transfer of impurities from PNaMTFSI to PEO, which may act as nucleating agents for PEO.[35]

The spherulitic growth rate depends on the energy required to transport the polymer chains to the surface of the growing crystal and also on the energy barrier for the creation of secondary nuclei of critical sizes. These energies depend on the molecular characteristics of the polymers and on the quantities T_m, T_c, and T_g.[36,37] As observed by DSC, PEO and PNaMTFSI are miscible and the incorporation of an amorphous miscible polymer causes a reduction in the equilibrium melting temperature (T_m^0).[38]

Figure 4a shows the growth rate of PEO spherulites as a function of the crystallization temperature measured using PLOM, and these values correspond to secondary nucleation

https://doi.org/10.1021/acs.energyfuels.2c04296
Energy Fuels 2023, 37, 5519−5529

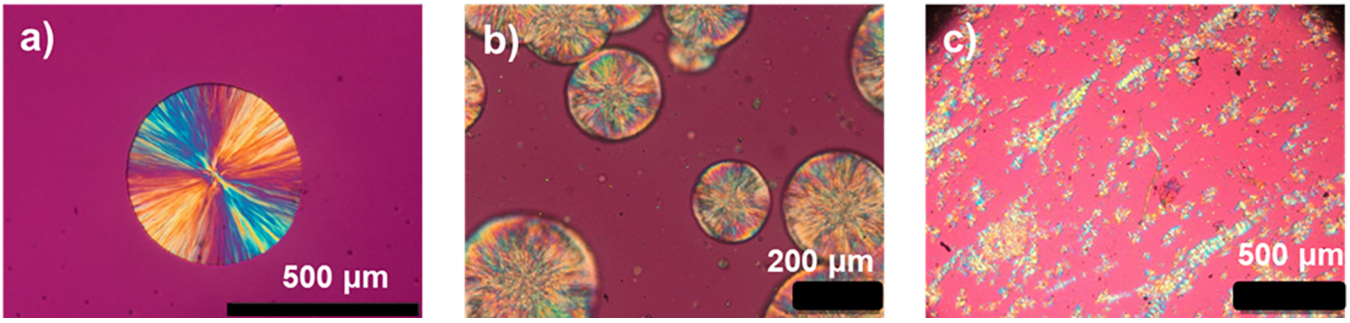

Figure 3. (a) Spherulite of neat PEO and (b) PEO spherulites in the 85/15 PEO/PNaMTFSI blend and (c) in the 70/30 PEO/PNaMTFSI blend.

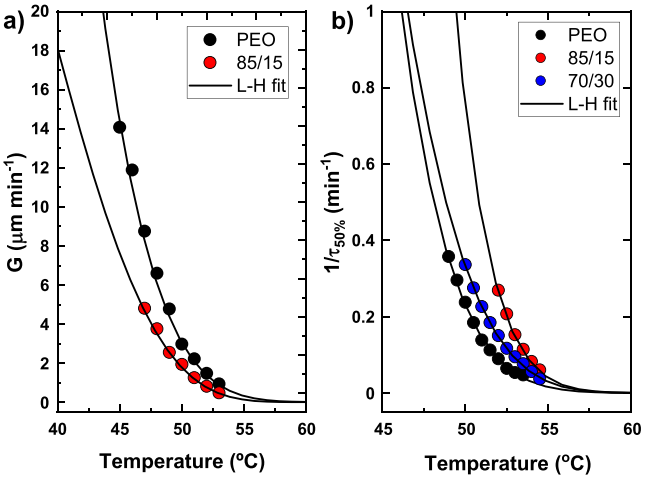

Figure 4. (a) Growth rate measured by PLOM and (b) overall crystallization rate measured by isothermal crystallization experiments in DSC. The solid lines are fits to the Lauritzen and Hoffman equation (see the Supporting Information), which are shown to guide the eye.

or growth rate kinetics only (i.e., they are independent of primary nucleation).

In the case of the 70/30 blend, it was impossible to determine the growth rates as the spherulites were too small because of the high nucleation density, and determining the variation in size as a function of time was not possible.

In polymers crystallized from the melt, the spherulitic growth rate versus crystallization temperature is a bell-shaped curve with a maximum between T_g and T_m. The left side of the graph is dominated by chain diffusion with a minor contribution from secondary nucleation; the right side of the curve is dominated by secondary nucleation with a minor contribution from diffusion. Figure 4a shows a decrease in the spherulitic growth rate of PEO when 15 wt % PNaMTFSI is incorporated in the blend (blend 85/15), indicating that the stiffer PNaMTFSI chains are interfering with the growth process of PEO spherulites, slowing it down. This change in the PEO spherulitic growth rate by the addition of the amorphous PNaMTFSI in a relatively small proportion (15 wt %) can be considered evidence of miscibility. If the blends were immiscible, the growth rate would have been most probably unaffected.

A different behavior occurs if primary nucleation is taken into account. The overall crystallization rate measured by DSC takes into account primary nucleation and secondary nucleation (growth). Figure 4b shows the inverse of the half-crystallization time ($1/\tau_{50\%}$) as a function of the crystallization temperature (T_c). The inverse of the half-crystallization time ($1/\tau_{50\%}$) is directly proportional to the overall crystallization rate.[26,37] In this case, the PEO overall crystallization rate increases with 15 wt % PNaMTFSI addition (blend 85/15) and then decreases when 30 wt % PNaMTFSI is added to the blend (70/30). Although, in both cases, the overall crystallization rate is higher than neat PEO, there is competition between nucleation and growth. As shown in Figure 3, the nucleation density increases with PNaMTFSI addition; this usually implies that the nucleation rate also increases. However, as seen in Figure 4a, the growth rate decreased with 15% PNaMTFSI addition, and it is expected that it will decrease even more with 30% addition as the T_g of the blend also increases (the concentration of PEO decreases). The results of Figure 4b can be explained by the competition between primary nucleation and growth. For 15% PNaMTFSI addition, the increase in nucleation dominates the overall crystallization kinetics, but with 30 wt % addition, the growth is the dominant factor.

3.3. Ionic Conductivity and Sodium-Ion Transference Number (t_{Na^+}).

The ionic conductivity is one of the most critical parameters to be considered for a solid electrolyte that shows potential to be used in a battery. Figure 5 presents the ionic conductivity of the blends as a function of the temperature. It is observed that the highest conductivity values are obtained at high temperatures for the electrolytes 85/15 and 70/30 (4.9×10^{-5} and 3.8×10^{-5} S cm^{-1} at 70 °C, respectively). When decreasing the temperature to 50 °C,

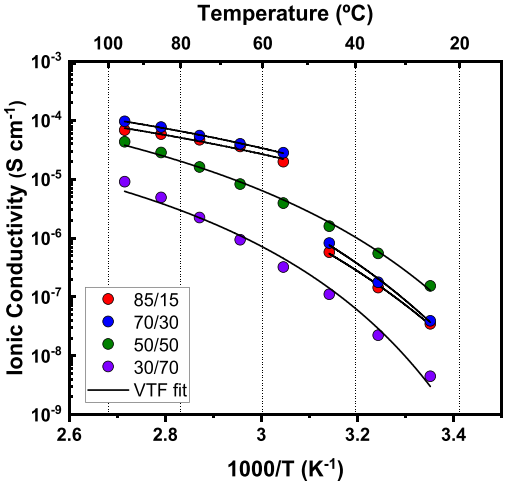

Figure 5. Ionic conductivity as a function of the temperature for the different electrolytes; the black lines are fits to the VTF equation.

https://doi.org/10.1021/acs.energyfuels.2c04296
Energy Fuels 2023, 37, 5519−5529

these same electrolytes present a drop in the ionic conductivity due to the crystallization of PEO. The electrolytes 50/50 and 30/70 do not present this drop in conductivity because they are completely amorphous, but the conductivity values are lower than those of the electrolytes with a lower PNaMTFSI concentration (1.2×10^{-5} and 1.5×10^{-6} S cm^{-1}at 70 °C, respectively). At higher contents of PNaMTFSI, the T_g of the blend increases, which brings forward that the mobility of the cations is restricted.

The VTF equation describes the behavior of the bent conductivity. It explains that diffusion can only occur when the diffusing particle (in this case, the sodium cation) moves from one free volume to another. The quantity $T - T_0$ gives the availability of the free volume.[9,39]

Table 1 presents the fitting parameters of the VTF equation (eq 3); the value of A is the prefactor of the equation, which

Table 1. Parameters Obtained by Fitting the Data with the VTF Equation for the Different Electrolytes

sample	A	E_a (kJ mol^{-1})	T_0 (K)	R^2
85/15 melted	3.49×10^{-3}	6.174	178.5	0.959
85/15 crystallized	28.93	20.61	178.5	0.999
70/30 melted	8.24×10^{-3}	6.758	185.7	0.997
70/30 crystallized	94.42	20.46	185.7	0.999
50/50	5.85×10^{-2}	9.831	204.23	0.998
30/70	4.95×10^{-2}	10.364	223.55	0.999

represents the theoretical ionic conductivity at very high temperatures. In this case, due to the mathematical adjustment, it is observed that, for the 85/15 and 70/30 materials at low temperatures (where PEO is crystallized), the slope is larger in the adjustment line, which makes the value of A very high. The most important parameter that can be calculated by this equation is the activation energy. It is observed in Table 1 that the lowest activation energies are for the 85/15 and 70/30 electrolytes at high temperatures (where PEO is molten), and their values are very similar. This makes sense since the ionic conductivity values between 50 and 100 °C are also very similar. When the PEO crystallizes, the activation energy becomes higher, increasing from 6 to 20 kJ mol^{-1} in the case of the 50/50 and 30/70 electrolytes. The values for these samples could be adjusted in all the temperature ranges since they are completely amorphous, and for these electrolytes, the activation energies are 9.831 and 10.364 kJ mol^{-1}. T_0 values were calculated as $T_g - 50$ °C for all electrolytes. In the case of the 50/50 and 30/70 compositions, they were taken directly from the values obtained by the non-isothermal DSC runs, but in the case of the 85/15 and 70/30 electrolytes, the T_g values were obtained by means of the Gordon-Taylor equation (Figure 2b).

One of the objectives of anchoring the anion to the polymer backbone is to allow solely cation transport (sodium in this case) so that a high sodium transference number value (t_{Na^+}), close to unity, is obtained. It has already been observed that not only the ionic conductivity but also a high sodium transference number is critical for a good electrochemical performance.[40] Different methods can be used to determine t_{Na^+} such as the electrochemical polarization method or diffusivity measurements. In this work, the t_{Na^+} was measured using the Bruce and Vincent method.[32] These experiments were done at 70 °C to provide enough ionic conductivity. Table S1 shows t_{Na^+} values measured for the different electrolytes 85/15, 70/30, and 50/50. The use of the PNaMTFSI leads to obtaining PEs displaying high t_{Na^+} in all the cases of above 0.83. This reflects the unique single-ion nature of these electrolytes where the only mobile species is the cation. These sodium-ion transference number values and the total ionic conductivity (σ_{total}) were used to calculate the sodium ion conductivity (σ_{Na^+}) (Figure 6). Remarkably, the

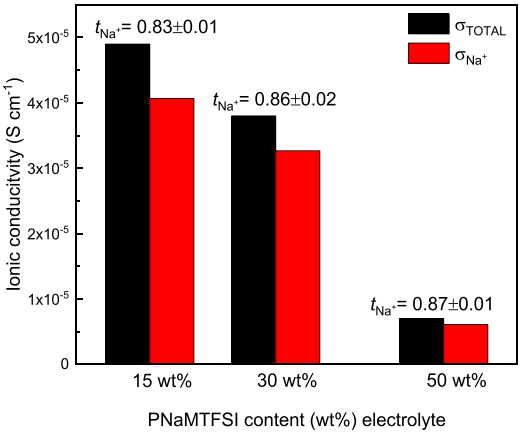

Figure 6. Sodium transference number, total ionic conductivity, and sodium ion conductivity of blends 85/15, 70/30, and 50/50 (15, 30, and 50 wt % PNaMTFSI) at 70 °C.

σ_{Na^+} is very similar to the total due to the high sodium transference number, meaning that the main contribution to the ionic conductivity comes from the Na ion, avoiding the undesired effects derived from the mobility of the anion that could lead to cell polarization, dendrite growth, and ultimately, cell failure.[41,42]

3.4. Electrochemical Stability with the Sodium Metal.

The temperature dependence of the sodium interfacial resistance was evaluated using electrochemical impedance spectroscopy (EIS) in Na^0|PE| Na^0 symmetrical cells (Figure 7a–c). Figure 7a shows the Nyquist plot of the four electrolyte compositions with different PNaMTFSI contents at 70 °C where a higher content of the single-ion conducting polymer in the electrolyte is translated into an increase of the total interfacial resistance (R_{int} = 7477 Ω cm^2 (15 wt %), R_{int} = 1747 Ω cm^2 (30 wt %), R_{int} = 17,459 Ω cm^2 (50 wt %), and R_{int} = 547,312 Ω cm^2 (70 wt %)). This could be ascribed to the lower ionic conductivity of such electrolytes. In addition, the temperature dependence of the sodium interfacial resistance was evaluated using EIS in Na^0|PE|Na^0 symmetrical cells for the 15 and 30 wt % PNaMTFSI-containing electrolytes (Figure 7b,c). In both cases, the bulk resistance and interfacial resistance increase when decreasing the temperature from 70 to 40 °C. This is due to the drop in the ionic conductivity when decreasing the temperature and, in addition, the poorer contact between the sodium metal and the electrolyte, leading to a higher resistive interface. In Figures S3–S5, the Nyquist diagrams are presented to show the results at low resistances.

The anodic stability of developed electrolytes was assessed by LSV. Figure 7d shows the LSV traces measured at 70 °C for all the different compositions. The increasing concentration of the PNaMTFSI improves the stability of the electrolyte from 3.5 (15 wt % PNaMTFSI) to 4.5 V versus Na^+/Na^0 (70 wt % PNaMTFSI). This could be explained by the lower oxidation stability of the ethylene oxide units of PEO compared with PNaMTFSI, so the electrolyte containing 70 wt % PNaMTFSI

https://doi.org/10.1021/acs.energyfuels.2c04296
Energy Fuels 2023, 37, 5519–5529

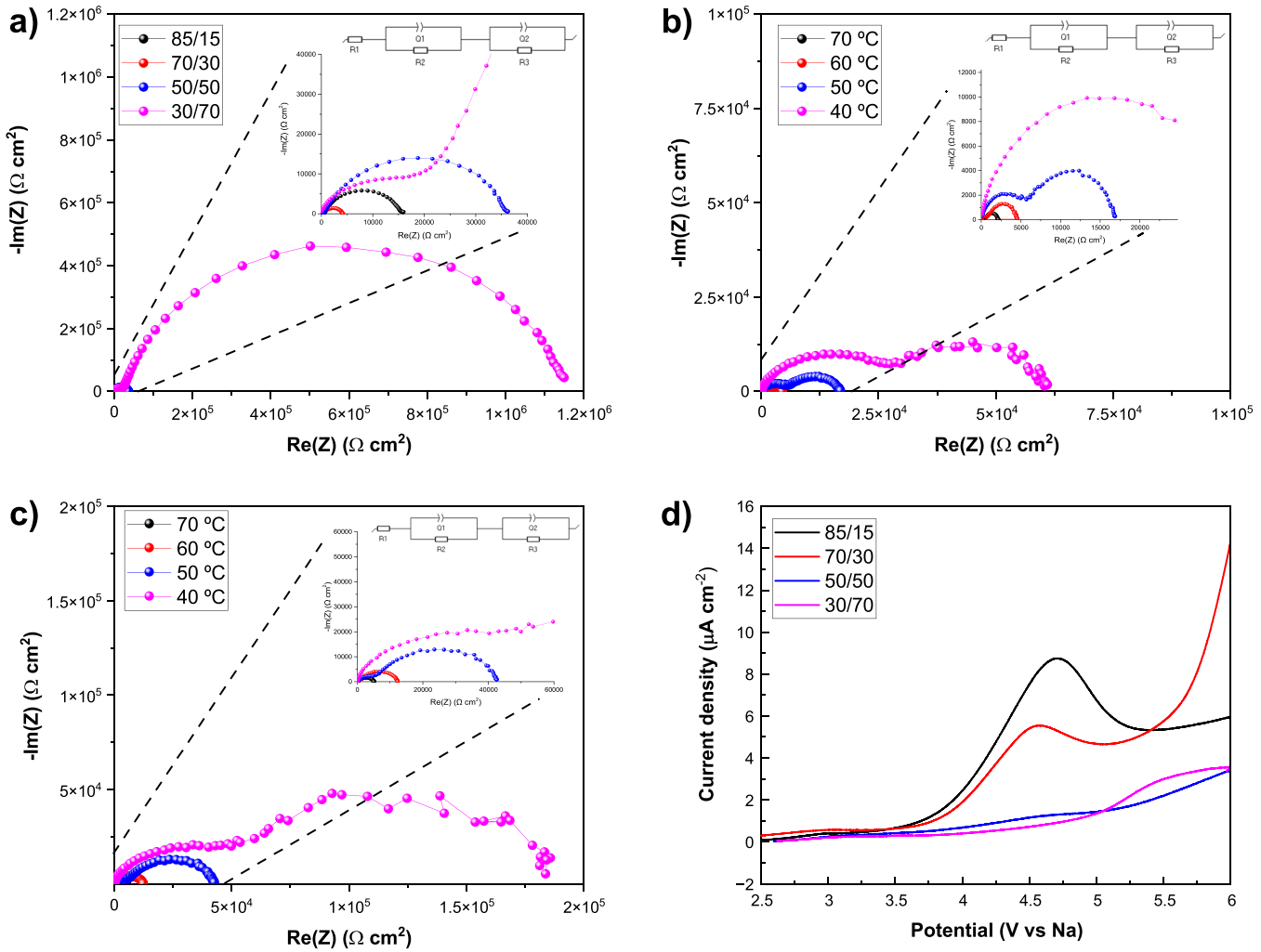

Figure 7. (a) Interfacial resistance of the 15, 30, 50, and 70 wt % PNaMTFSI-containing electrolytes at 70 °C. (b) Nyquist plot of the 15 wt % PNaMTFSI-containing electrolytes at different temperatures. (c) Nyquist plot of the 30 wt % PNaMTFSI-containing electrolytes at different temperatures. (d) LSV of the 4 different-composition electrolytes at 70 °C.

is the electrolyte with the highest oxidation stability. These results prove the potential application of these electrolytes to be used with <4.0 V class cathode materials, such as sodium iron phosphate ($NaFePO_4$).[43,44]

Figure 8 shows the overall stability window for the electrolyte 70/30 (30 wt % PNaMTFSI), being the composition with the highest ionic conductivity at 70 °C (3.8×10^{-5} S cm^{-1}). During the cathodic scan, reversible peaks at −1 and 0.5 V versus Na^+/Na^0 can be observed corresponding to the sodium plating and striping; moreover, the Coulombic efficiency of the plating/striping process was calculated, showing excellent values close to 100%. In addition, the anodic limit of the electrolyte was found to be approximately 4 V versus Na^+/Na^0. All this data confirm the good performance of these materials to support the sodium chemistry.

3.5. Comparison of Sodium and Lithium Solid Polymer Electrolytes. In this section, a comparison is made between the sodium electrolytes reported in this work with the lithium electrolytes reported by our group previously.[22] This comparison is made to evaluate the effect of the cation on the overall properties of the blends since, in both cases for lithium and sodium, the same polymers with equal molecular weights were employed.

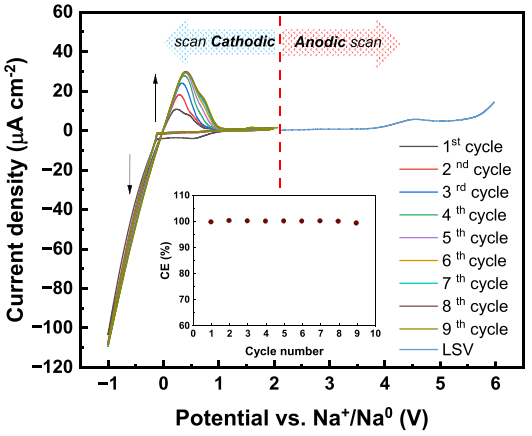

Figure 8. Electrochemical stability window obtained by CV at 1 mV s^{-1} for 30 wt % PNaMTFSI at 70 °C.

Figure 9a presents the change in the T_g of the blends as a function of the fraction of PEO in the blend. It is observed that the data for the two systems are adjusted to the Gordon-Taylor equation where the parameter k is taken into account, which is related to the changes in the expansion coefficient. In both

https://doi.org/10.1021/acs.energyfuels.2c04296
Energy Fuels 2023, 37, 5519−5529

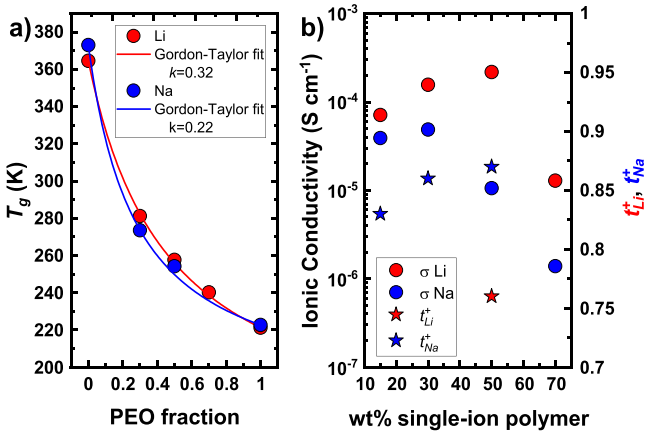

Figure 9. Comparison of PEO/PXMTFSI blends where X = Li or Na. (a) T_g as a function of the PEO fraction. (b) Ionic conductivity and ion transference number as a function of the single-ion polymer content in the blend.

cases, there is a negative deviation from a simple mixing rule of T_g with the composition; however, the stronger intermolecular interactions between PEO and PLiMTFSI increase the T_g of the blend more than in blends with PNaMTFSI.[45−47] In addition, as the cation size increases, the separation between the polymer chains increases, so the T_g of the sodium mixtures is lower.[48]

The ionic conductivity in solid polymer electrolytes is directly related to the number of free carriers as well as their mobility, according to the equation

$$\sigma = \sum z_i n_i \mu_i \tag{6}$$

where z_i, n_i, and μ_i are the ion charge, number of charge carriers, and ion mobility, respectively.

Figure 9b shows that the ionic conductivity in Li electrolytes is higher than in the case of Na electrolytes. This can be explained by the fact that the local viscous force (of cations moving in the media) increases with increasing the cation size, which reduces the cation conduction,[48] and hence, a larger cation such as Na will conduct less than a smaller one such as lithium. A similar effect where, in the same polymer matrices, there is a higher ionic conductivity with lithium than with sodium salts has been previously reported.[49] The values of ion transference numbers for both systems are also presented, and it is observed that the values of the transference number are higher in the sodium system perhaps because this system has a lower T_g.

The spherulitic growth rate of the blends can be normalized by dividing the value of G by G_{PEO}, giving values of 1 for PEO. Figure 10a shows the relationship between the spherulitic growth rate of the sample with respect to PEO, and in this case, it is clearly observed that, in both cases, the spherulitic growth rate decreases with both cations, that is, 90% with Li and 40% with Na, for the blend with 15 wt % single-ion polymer electrolyte. This indicates that the growth rate of PEO crystals is more affected when the single-ion polymer has lithium cations. This is a consequence of the stronger intermolecular interactions in the PEO/PLiMTFSI blends in comparison with the PEO/PNaMTFSI blends. When the PEO chains in the miscible mixed melt with PLiMTFSI chains crystallize by attaching to a growing PEO spherulite, they have to diffuse away from the PLiMTFSI chains. This process is more difficult when the intermolecular interactions are stronger as in the case of PEO/PLiMTFSI blends in comparison to PEO/PNaMTFSI blends, hence the stronger suppression of the spherulitic growth rate.

On the other hand, if we plot the overall crystallization rate $(1/\tau_{50\%})$ of each electrolyte divided by the overall crystallization rate of PEO $(1/\tau_{50\%,PEO})$ as a function of the crystallization temperature (Figure 10b), it is observed that, for the case of lithium blends, the overall crystallization rate decreases to less than 50% with 15 and 30 wt % PLiMTFSI, but for the case of sodium electrolytes, the crystallization rate increases up to 3 times more with 15 wt % PNaMTFSI and 1.5 times more with 30 wt % PNaMTFSI. A clear difference is

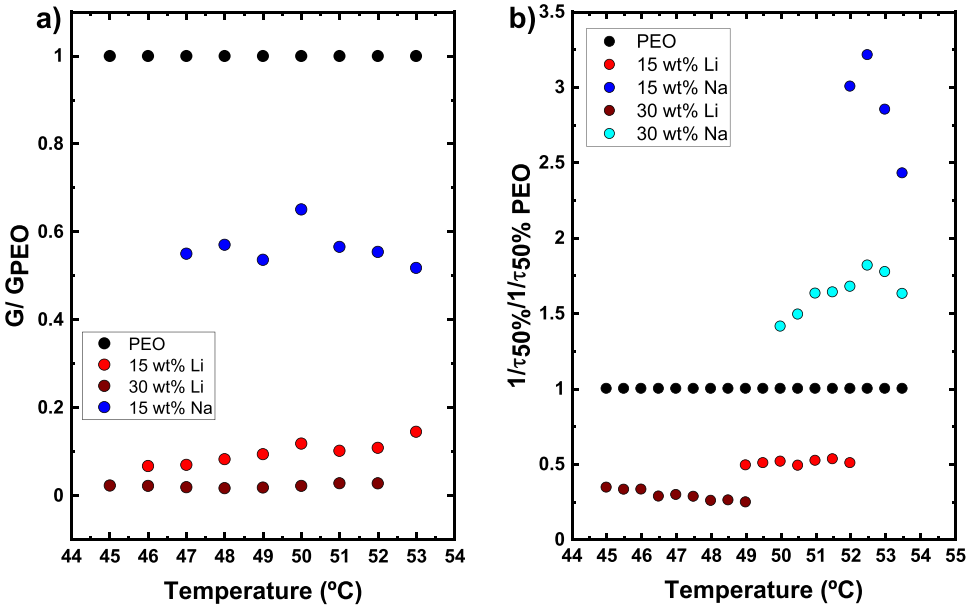

Figure 10. (a) Growth rates and (b) overall crystallization rates normalized by the neat PEO data for the lithium and sodium electrolytes as a function of the crystallization temperature.

https://doi.org/10.1021/acs.energyfuels.2c04296
Energy Fuels 2023, 37, 5519−5529

observed in how the crystallization of PEO is affected with different cations.

It should be remembered that the overall crystallization rate determined by DSC takes into account both primary nucleation and growth. As discussed in Section 3.2, in electrolytes with sodium, there is a higher nucleation density in comparison to those with lithium. Therefore, in the case of PEO/PLiMTFSI blends, the growth rate is the dominant term of the overall crystallization kinetics, causing its depression. Instead, for PEO/PNaMTFSI, it is the primary nucleation that dominates the kinetics, and it provokes an increase in the overall crystallization kinetics, leading to very different trends between electrolytes with Li or Na as shown in Figure 10b.

4. CONCLUSIONS

In this article, high-conducting single-ion solid polymer electrolytes were presented based on polyethylene oxide/sodium sulfonamide polymethacrylate blends. Four different blends of single-sodium-ion polymers based on PEO and PNaMTFSI were prepared (15, 30, 50, and 70 wt % PNaMTFSI). Non-isothermal DSC showed that the crystallinity of PEO decreases as a function of the concentration of PNaMTFSI, being completely amorphous with 50 wt % PNaMTFSI. Moreover, a single intermediate T_g is presented between PEO and PNaMTFSI, proving the miscibility of these two polymers. In addition, the ionic conductivity was determined for the electrolytes and correlated to the DSC results with the electrolytes with 15 and 30 wt % PNaMTFSI being the ones that showed the highest ionic conductivity (in the order of 10^{-5} S cm^{-1} at 70 °C). Sodium-ion transference number values of greater than 0.83 were obtained, confirming the single-ion conduction property. As expected for miscible blends, both the spherulitic growth rate and the overall crystallization rate were a function of the blend composition. All the electrolytes showed stability of higher than 4 V, which opens the possibility of their use in sodium metal batteries. A comparison was made between the effect of lithium or sodium in the same polymeric system, and it was shown that the ionic conductivity in sodium electrolytes is a little less because the local viscous force increases with increasing the cation size. Finally, the effect of the cation on the crystallization of PEO was studied where lithium decreases the crystallization rate of PEO more, while the presence of sodium has a greater nucleating effect on PEO, which increases the overall crystallization rate with respect to neat PEO.

■ ASSOCIATED CONTENT

Supporting Information

The Supporting Information is available free of charge at https://pubs.acs.org/doi/10.1021/acs.energyfuels.2c04296.

Characterization of PNaMTFSI, equations for the Lauritzen-Hoffman (L-H) fit, data for the calculation of the sodium-ion transference number (t_{Na^+}), the storage modulus as a function of the temperature for the different compositions, and the different electrochemical impedance spectroscopy spectra as a function of the temperature (PDF)

■ AUTHOR INFORMATION

Corresponding Authors

Alejandro J. Müller − *POLYMAT and Department of Polymers and Advanced Materials: Physics, Chemistry and Technology, Faculty of Chemistry, University of the Basque Country UPV/EHU, 20018 Donostia-San Sebastián, Spain; IKERBASQUE, Basque Foundation for Science, 48009 Bilbao, Spain;* orcid.org/0000-0001-7009-7715; Email: alejandrojesus.muller@ehu.es

David Mecerreyes − *POLYMAT and Department of Polymers and Advanced Materials: Physics, Chemistry and Technology, Faculty of Chemistry, University of the Basque Country UPV/EHU, 20018 Donostia-San Sebastián, Spain; IKERBASQUE, Basque Foundation for Science, 48009 Bilbao, Spain;* orcid.org/0000-0002-0788-7156; Email: david.mecerreyes@ehu.es

Authors

Jorge L. Olmedo-Martínez − *POLYMAT and Department of Polymers and Advanced Materials: Physics, Chemistry and Technology, Faculty of Chemistry, University of the Basque Country UPV/EHU, 20018 Donostia-San Sebastián, Spain*

Asier Fdz De Anastro − *Centre for Cooperative Research on Alternative Energies (CIC energiGUNE), Basque Research and Technology Alliance (BRTA), 01510 Vitoria-Gasteiz, Spain*

María Martínez-Ibañez − *Centre for Cooperative Research on Alternative Energies (CIC energiGUNE), Basque Research and Technology Alliance (BRTA), 01510 Vitoria-Gasteiz, Spain*

Complete contact information is available at: https://pubs.acs.org/10.1021/acs.energyfuels.2c04296

Author Contributions

The manuscript was written through contributions of all authors. All authors have given approval to the final version of the manuscript.

Notes

The authors declare no competing financial interest.

■ ACKNOWLEDGMENTS

We acknowledge the funding by Agencia Estatal de Investigación (no. PLEC2021-007929). This work has received funding from the Basque Government through grant no. IT1503-22.

■ REFERENCES

(1) Armand, M.; Tarascon, J.-M. Building Better Batteries. *Nature* **2008**, *451*, 652−657.

(2) Kim, S.-W.; Seo, D.-H.; Ma, X.; Ceder, G.; Kang, K. Electrode Materials for Rechargeable Sodium-ion Batteries: Potential Alternatives to Current Lithium-ion Batteries. *Adv. Energy Mater.* **2012**, *2*, 710−721.

(3) Xu, W.; Wang, J.; Ding, F.; Chen, X.; Nasybulin, E.; Zhang, Y.; Zhang, J. G. Lithium Metal Anodes for Rechargeable Batteries. *Energy Environ. Sci.* **2014**, *7*, 513−537.

(4) Nayak, P. K.; Yang, L.; Brehm, W.; Adelhelm, P. From Lithium-ion to Sodium-ion Batteries: Advantages, Challenges, and Surprises. *Angew. Chem., Int. Ed.* **2018**, *57*, 102−120.

(5) Wang, Y.; Wang, Y.; Wang, Y.-X.; Feng, X.; Chen, W.; Ai, X.; Yang, H.; Cao, Y. Developments and Perspectives on Emerging High-Energy-Density Sodium-Metal Batteries. *Chem* **2019**, *5*, 2547−2570.

(6) Yang, J.; Zhang, H.; Zhou, Q.; Qu, H.; Dong, T.; Zhang, M.; Tang, B.; Zhang, J.; Cui, G. Safety-Enhanced Polymer Electrolytes for Sodium Batteries: Recent Progress and Perspectives. *ACS Appl. Mater. Interfaces* **2019**, *11*, 17109−17127.

(7) Lee, B.; Paek, E.; Mitlin, D.; Lee, S. W. Sodium Metal Anodes: Emerging Solutions to Dendrite Growth. *Chem. Rev.* **2019**, *119*, 5416−5460.
(8) Mindemark, J.; Lacey, M. J.; Bowden, T.; Brandell, D. Beyond PEO — Alternative Host Materials for Li^+ -Conducting Solid Polymer Electrolytes. *Prog. Polym. Sci.* **2018**, *81*, 114−143.
(9) Ratner, M. A.; Johansson, P.; Shriver, D. F. Polymer Electrolytes: Ionic Transport Mechanisms and Relaxation Coupling. *MRS Bull.* **2000**, *25*, 31−37.
(10) Jeong, K.; Park, S.; Lee, S.-Y. Revisiting Polymeric Single Lithium-Ion Conductors as an Organic Route for All-Solid-State Lithium Ion and Metal Batteries. *J. Mater. Chem. A* **2019**, *7*, 1917−1935.
(11) Nederstedt, H.; Jannasch, P. Single-Ion Conducting Polymer Electrolytes with Alternating Ionic Mesogen-like Moieties Interconnected by Poly (Ethylene Oxide) Segments. *Polymer* **2019**, *177*, 231−240.
(12) Vahini, M.; Muthuvinayagam, M. Synthesis and Electrochemical Studies on Sodium Ion Conducting PVP Based Solid Polymer Electrolytes. *J. Mater. Sci.: Mater. Electron.* **2019**, *30*, 5609−5619.
(13) Verma, H.; Mishra, K.; Rai, D. K. Sodium Ion Conducting Nanocomposite Polymer Electrolyte Membrane for Sodium Ion Batteries. *J. Solid State Electrochem.* **2020**, *24*, 521−532.
(14) Chauhan, A. K.; Mishra, K.; Kumar, D.; Singh, A. Enhancing Sodium Ion Transport in a PEO-Based Solid Polymer Electrolyte System with NaAlO2 Active Fillers. *J. Electron. Mater.* **2021**, *50*, 5122−5133.
(15) Gebert, F.; Knott, J.; Gorkin, R., III; Chou, S.-L.; Dou, S.-X. Polymer Electrolytes for Sodium-Ion Batteries. *Energy Storage Mater.* **2021**, *36*, 10−30.
(16) Li, J.; Zhu, H.; Wang, X.; Armand, M.; MacFarlane, D. R.; Forsyth, M. Synthesis of Sodium Poly [4-Styrenesulfonyl (Trifluoromethylsulfonyl) Imide]-Co-Ethylacrylate] Solid Polymer Electrolytes. *Electrochim. Acta* **2015**, *175*, 232−239.
(17) Liu, K.; Xie, Y.; Yang, Z.; Kim, H.-K.; Dzwiniel, T. L.; Yang, J.; Xiong, H.; Liao, C. Design of a Single-Ion Conducting Polymer Electrolyte for Sodium-Ion Batteries. *J. Electrochem. Soc.* **2021**, *168*, 120543.
(18) Villaluenga, I.; Bogle, X.; Greenbaum, S.; de Muro, I. G.; Rojo, T.; Armand, M. Cation Only Conduction in New Polymer−SiO_2 Nanohybrids: Na^+ Electrolytes. *J. Mater. Chem. A* **2013**, *1*, 8348−8352.
(19) Blatt, M. P.; Hallinan, D. T., Jr. Polymer Blend Electrolytes for Batteries and Beyond. *Ind. Eng. Chem. Res.* **2021**, *60*, 17303−17327.
(20) Doyle, R. P.; Chen, X.; Macrae, M.; Srungavarapu, A.; Smith, L. J.; Gopinadhan, M.; Osuji, C. O.; Granados-Focil, S. Poly (Ethylenimine)-Based Polymer Blends as Single-Ion Lithium Conductors. *Macromolecules* **2014**, *47*, 3401−3408.
(21) Deng, F.; Wang, X.; He, D.; Hu, J.; Gong, C.; Ye, Y. S.; Xie, X.; Xue, Z. Microporous Polymer Electrolyte Based on PVDF/PEO Star Polymer Blends for Lithium Ion Batteries. *J. Membr. Sci.* **2015**, *491*, 82−89.
(22) Olmedo-Martínez, J. L.; Porcarelli, L.; Alegría, Á.; Mecerreyes, D.; Müller, A. J. High Lithium Conductivity of Miscible Poly-(Ethylene Oxide)/Methacrylic Sulfonamide Anionic Polyelectrolyte Polymer Blends. *Macromolecules* **2020**, *53*, 4442−4453.
(23) Olmedo-Martínez, J. L.; Porcarelli, L.; Guzmán-González, G.; Calafel, I.; Forsyth, M.; Mecerreyes, D.; Müller, A. J. Ternary Poly (Ethylene Oxide)/Poly (l, l-Lactide) PEO/PLA Blends as High-Temperature Solid Polymer Electrolytes for Lithium Batteries. *ACS Appl. Polym. Mater.* **2021**, *3*, 6326−6337.
(24) Shaplov, A. S.; Vlasov, P. S.; Armand, M.; Lozinskaya, E. I.; Ponkratov, D. O.; Malyshkina, I. A.; Vidal, F.; Okatova, O. V.; Pavlov, G. M.; Wandrey, C.; et al. Design and Synthesis of New Anionic "Polymeric Ionic Liquids" with High Charge Delocalization. *Polym. Chem.* **2011**, *2*, 2609.
(25) Porcarelli, L.; Aboudzadeh, M. A.; Rubatat, L.; Nair, J. R.; Shaplov, A. S.; Gerbaldi, C.; Mecerreyes, D. Single-Ion Triblock Copolymer Electrolytes Based on Poly(Ethylene Oxide) and Methacrylic Sulfonamide Blocks for Lithium Metal Batteries. *J. Power Sources* **2017**, *364*, 191−199.
(26) Lorenzo, A. T.; Arnal, M. L.; Albuerne, J.; Müller, A. J. DSC Isothermal Polymer Crystallization Kinetics Measurements and the Use of the Avrami Equation to Fit the Data: Guidelines to Avoid Common Problems. *Polym. Test.* **2007**, *26*, 222−231.
(27) Pérez-Camargo, R. A.; Liu, G.-M.; Wang, D.-J.; Müller, A. J. Experimental and Data Fitting Guidelines for the Determination of Polymer Crystallization Kinetics. *Chin. J. Polym. Sci.* **2022**, 658−691.
(28) Beaumont, R. H.; Clegg, B.; Gee, G.; Herbert, J. B. M.; Marks, D. J.; Roberts, R. C.; Sims, D. Heat Capacities of Propylene Oxide and of Some Polymers of Ethylene and Propylene Oxides. *Polymer* **1966**, *7*, 401−417.
(29) Kalogeras, I. M.; Brostow, W. Glass Transition Temperatures in Binary Polymer Blends. *J. Polym. Sci., Part B: Polym. Phys.* **2009**, *47*, 80−95.
(30) Schneider, H. A. The Gordon-Taylor Equation. Additivity and Interaction in Compatible Polymer Blends. *Makromol. Chem.* **1988**, *189*, 1941−1955.
(31) Diederichsen, K. M.; Buss, H. G.; McCloskey, B. D. The Compensation Effect in the Vogel−Tammann−Fulcher (VTF) Equation for Polymer-Based Electrolytes. *Macromolecules* **2017**, *50*, 3831−3840.
(32) Evans, J.; Vincent, C. A.; Bruce, P. G. Electrochemical Measurement of Transference Numbers in Polymer Electrolytes. *Polymer* **1987**, *28*, 2324−2328.
(33) Kisliuk, A.; Bocharova, V.; Popov, I.; Gainaru, C.; Sokolov, A. P. Fundamental Parameters Governing Ion Conductivity in Polymer Electrolytes. *Electrochim. Acta* **2019**, 191−196.
(34) Olmedo-Martínez, J. L.; Meabe, L.; Basterretxea, A.; Mecerreyes, D.; Müller, A. J. Effect of Chemical Structure and Salt Concentration on the Crystallization and Ionic Conductivity of Aliphatic Polyethers. *Polymer* **2019**, *11*, 452.
(35) Suzuki, Y.; Steinhart, M.; Kappl, M.; Butt, H.-J.; Floudas, G. Effects of Polydispersity, Additives, Impurities and Surfaces on the Crystallization of Poly (Ethylene Oxide)(PEO) Confined to Nanoporous Alumina. *Polymer* **2016**, *99*, 273−280.
(36) Michell, R. M.; Müller, A. J. Confined Crystallization of Polymeric Materials. *Prog. Polym. Sci.* **2016**, *54*, 183−213.
(37) Müller, A. J.; Michell, R. M.; Lorenzo, A. T. Isothermal Crystallization Kinetics of Polymers. In *Polymer Morphology: Principles, Characterization, and Processing*; Guo, Q., Ed.; John Wiley & Sons, 2016; pp. 181−203, DOI: 10.1002/9781118892756.ch11.
(38) Pereira, A. G. B.; Gouveia, R. F.; de Carvalho, G. M.; Rubira, A. F.; Muniz, E. C. Polymer Blends Based on PEO and Starch: Miscibility and Spherulite Growth Rate Evaluated through DSC and Optical Microscopy. *Mater. Sci. Eng. C* **2009**, 499.
(39) Agrawal, R. C.; Pandey, G. P. Solid Polymer Electrolytes: Materials Designing and All-Solid-State Battery Applications: An Overview. *J. Phys. D: Appl. Phys.* **2008**, *41*, No. 223001.
(40) Pan, Q.; Li, Z.; Zhang, W.; Zeng, D.; Sun, Y.; Cheng, H. Single Ion Conducting Sodium Ion Batteries Enabled by a Sodium Ion Exchanged Poly (Bis (4-Carbonyl Benzene Sulfonyl) Imide-Co-2, 5-Diamino Benzesulfonic Acid) Polymer Electrolyte. *Solid State Ionics* **2017**, *300*, 60−66.
(41) Youcef, H. B.; Orayech, B.; Del Amo, J. M. L.; Bonilla, F.; Shanmukaraj, D.; Armand, M. Functionalized Cellulose as Quasi Single-Ion Conductors in Polymer Electrolyte for All-Solid−State Li/Na and Li−S Batteries. *Solid State Ionics* **2020**, *345*, No. 115168.
(42) Hilder, M.; Howlett, P. C.; Saurel, D.; Gonzalo, E.; Basile, A.; Armand, M.; Rojo, T.; Kar, M.; MacFarlane, D. R.; Forsyth, M. The Effect of Cation Chemistry on Physicochemical Behaviour of Superconcentrated NaFSI Based Ionic Liquid Electrolytes and the Implications for Na Battery Performance. *Electrochim. Acta* **2018**, *268*, 94−100.
(43) Wongittharom, N.; Lee, T.-C.; Wang, C.-H.; Wang, Y.-C.; Chang, J.-K. Electrochemical Performance of Na/NaFePO4 Sodium-

Ion Batteries with Ionic Liquid Electrolytes. *J. Mater. Chem. A* **2014**, *2*, 5655−5661.
(44) Oh, S.-M.; Myung, S.-T.; Hassoun, J.; Scrosati, B.; Sun, Y.-K. Reversible NaFePO4 Electrode for Sodium Secondary Batteries. *Electrochem. Commun.* **2012**, *22*, 149−152.
(45) Aubin, M.; Prud'Homme, R. E. Analysis of the Glass Transition Temperature of Miscible Polymer Blends. *Macromolecules* **1988**, *21*, 2945−2949.
(46) Kadla, J. F.; Kubo, S. Miscibility and Hydrogen Bonding in Blends of Poly (Ethylene Oxide) and Kraft Lignin. *Macromolecules* **2003**, *36*, 7803−7811.
(47) Schneider, H. A. Glass Transition Behaviour of Compatible Polymer Blends. *Polymer* **1989**, *30*, 771−779.
(48) Arya, A.; Sharma, A. L. Electrolyte for Energy Storage/Conversion (Li+, Na+, Mg2+) Devices Based on PVC and Their Associated Polymer: A Comprehensive Review. *J. Solid State Electrochem.* **2019**, *23*, 997−1059.
(49) Xu, L.; Li, J.; Deng, W.; Li, L.; Zou, G.; Hou, H.; Huang, L.; Ji, X. Boosting the Ionic Conductivity of PEO Electrolytes by Waste Eggshell-Derived Fillers for High-Performance Solid Lithium/Sodium Batteries. *Mater. Chem. Front.* **2021**, *5*, 1315−1323.

https://doi.org/10.1021/acs.energyfuels.2c04296
Energy Fuels 2023, 37, 5519−5529